Measurement of Chromatic Aberrations Using Phase Retrieval

M. D. Bergkoetter,[1,2] B. E. Kruschwitz,[1,3] S.-W. Bahk,[3] and J. R. Fienup[1]

[1]The Institute of Optics, University of Rochester
[2]NASA Goddard Space Flight Center
[3]Laboratory for Laser Energetics, University of Rochester

Phase retrieval is a computational method for estimating the phase of an electromagnetic field based on measurements of the intensity in one or more planes. For wavefront-sensing applications, the phase of interest is in the pupil plane of an optical system, and typically the aperture and image-plane intensity from a point source [the point-spread function (PSF)] are known.[1] The iterative process of retrieving the phase involves forming an initial estimate of the wavefront in the pupil plane, simulating a propagation of that field to the image plane (which typically involves a Fourier transform), and comparing the resulting intensity distribution with the measured intensity via an error metric. The wavefront estimate is then modified to improve agreement in the image plane.

Among the various applications of this general approach is the improvement of diagnostic tools for the OMEGA EP laser. In this case, phase retrieval complements measurements provided by a conventional Shack–Hartmann wavefront sensor (SHWFS) with an estimate of non-common-path error and differential piston between regions of the segmented beam.[2] A proposed way to improve this system is to also estimate chromatic aberrations in the system. These can arise in a chirped-pulse–amplification laser such as OMEGA EP in the form of (1) residual angular dispersion from the pulse stretcher and compressor and (2) axial dispersion (longitudinal chromatic aberration) due to transmissive elements, both of which can lead to a significant reduction in the focused intensity.

We use a modal approach to modeling chromatic effects. Angular dispersion is modeled as a wavefront tilt that varies linearly with wavelength and longitudinal chromatic aberration as a defocus that varies linearly with wavelength. By forcing the spectrally varying components of the wavefronts to fit this model, we can mitigate uniqueness problems that would arise if they were allowed to vary independently. In our model, we assume that (1) there is an initial estimate of the monochromatic wavefront W_0 measured by a SHWFS and (2) there is also a non-common-path error between the SHWFS and the focusing optics, which must be estimated in terms of a monochromatic wavefront W_M, in addition to the chromatic aberrations $(\lambda–\lambda_\mathrm{r})\, W_\mathrm{c}$, relative to a reference wavelength λ_r, so that

$$W(\xi,\eta) = W_0(\xi,\eta) + W_\mathrm{M}(\xi,\eta) + (\lambda - \lambda_\mathrm{r}) W_\mathrm{c}(\xi,\eta), \tag{1}$$

where $W_\mathrm{M}(\xi,\eta) \equiv \sum_{n=0}^{N} a_n Z_n(\xi,\eta)$ and $W_\mathrm{c}(\xi,\eta) \equiv \sum_{n=0}^{N} c_n Z_n(\xi,\eta)$.

Having mentioned above "differential piston between regions of the segmented beam,"[2] this model does not capture the segment-to-segment errors that can exist from a tiled grating. The a_n and c_n coefficients would usually vary from segment to segment (including piston tip and tilt).

In Eq. (1), ξ and η are pupil-plane coordinates, λ is the wavelength of a single spectral component, and Z_n is the nth Zernike polynomial. The phase-retrieval algorithm jointly estimates the unknown monochromatic wavefront along with the chromatic

aberrations in terms of the sets of coefficients a_n and c_n, respectively. The exit pupil amplitude is assumed to be a known aperture with transmittance $P(\xi, \eta)$, and each spectral component is given a scalar amplitude weight, based on the known power spectrum. Each spectral component is propagated from the pupil plane to the image plane separately, and the total PSF in the image plane is the incoherent sum of the spectral components. The error metric is the normalized sum-squared difference between the simulated and measured PSF's.

As a simple test case, we simulated PSF's with angular dispersion of 1.2 waves peak-to-valley (p–v) of tip/tilt and axial dispersion of 1 wave of defocus, both across an 8-nm bandwidth. Besides the global minimum, three local minima also appear, where one or both of the signs of the dispersion parameters are reversed. When a known defocus is added, two of the local minima disappear and the error metric appears as in Fig. 1(a).

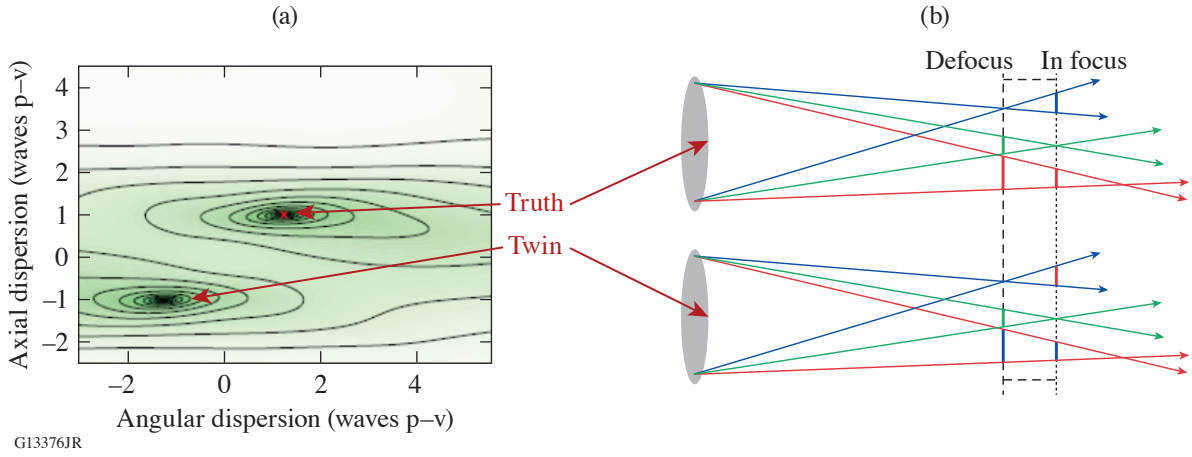

Figure 1
The twin image problem is illustrated. (a) Error metric as a function of the two dispersion variables, with a known defocus included. The global minimum (correct values) is in the center of the plot at coordinates (1.2, 1). (b) Illustration of how defocus does not eliminate the joint axial–angular twin.

We can explain the appearance of these minima and their relation with defocus by analogy to the well-known twin image problem in monochromatic phase retrieval, which arises because the absolute value of the Fourier transform of any complex signal $f(u)$ is the same as that of its complex conjugate flipped about the origin $f^*(-u)$. Defocus cannot eliminate the joint axial–angular twin, when the signs of both the angular and axial dispersion are reversed simultaneously. This effect can be visualized with the ray trace in Fig. 1(b), which shows axial dispersion causing each spectral component to focus at a different horizontal position and angular dispersion causing the focal points to spread vertically.

However, the PSF produced by the twin is subtly different due to the scaling effect of the wave number $2\pi/\lambda$ in the complex exponential and any asymmetry in the spectrum. If this results in a significantly higher error metric for the twin than the true solution, a sufficient strategy for avoiding this minimum is to check the error metric against a threshold value after the optimizer converges; if it is too high, reverse the signs of the dispersion coefficients and perform another round of local nonlinear optimization to confirm whether that minimizes the error metric.

To test this strategy, the algorithm was run through a series of trials with a variety of simulated true reference wavefronts and various starting guesses for the dispersion parameters. In all cases, the true chromatic aberrations were 1.2 waves p–v of angular dispersion and 1 wave p–v of axial dispersion across an 8-nm bandwidth (or equivalently stated as 0.15 waves/nm and 0.125 waves/nm, respectively). The spectral weights for intensity were representative of measured spectra in fully amplified shots on OMEGA EP [shown in Fig. 2(a)]. Each of the randomized true reference wavefronts was the sum of a known part W_0 with a magnitude 0.4 waves rms and an unknown part W_M [simulating non-common-path error, an example of which is shown in Fig. 2(b)] that had to be retrieved and had a magnitude of 0.11 waves rms. Known defocus in the amount of 1.5 waves was also added.

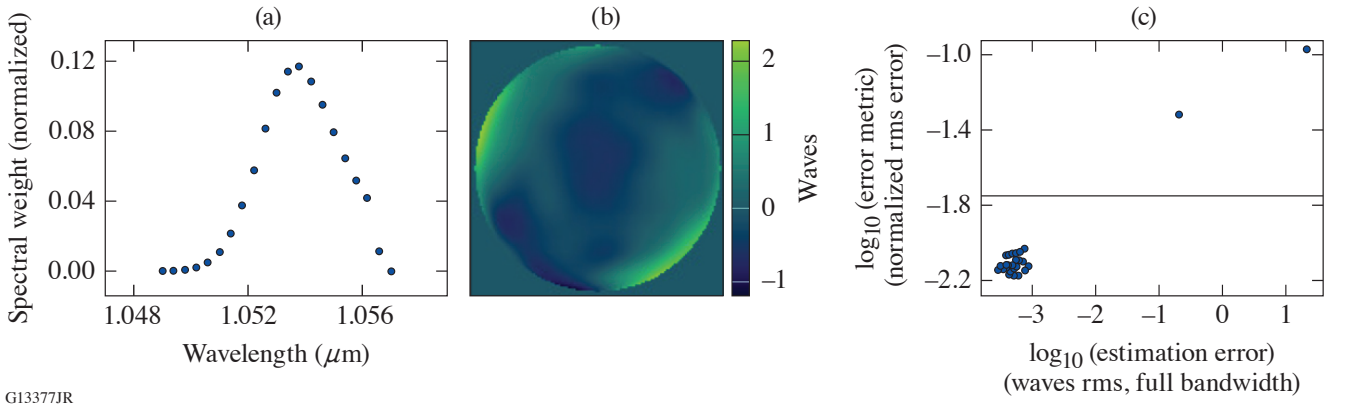

Figure 2
Monte Carlo simulation results: (a) Intensity spectrum used in Monte Carlo simulations; (b) representative example of random monochromatic wavefront aberration (defocus removed); and (c) resulting phase-retrieval error metric versus error of the reconstruction, where the error is computed over the full bandwidth. Successful cases in (c) have a low estimation error, and failed cases are identifiable by a large error metric in the PSF fit. Cases above the vertical line are considered failed cases.

Both the unknown part of the monochromatic reference wavefront and the dispersion terms were retrieved. A bootstrapping process was used in which the monochromatic reference wavefront was optimized alone while the dispersion terms were left at zero. Once that converged, a second stage was carried out, allowing both the monochromatic and dispersion terms to vary. In combination with the twin phase check described earlier, this strategy was successful in all but two of the 1600 tested cases. In the failed cases, the normalized root-mean-squared error between the estimated and true PSF's was about 10× greater than the error metric for successful cases, as shown by the outliers in Fig. 2(c). Therefore, if one of these failures occurs in practice, it can be recognized by the large residual error metric and recovered from by performing another optimization run from a different random starting point.

To test the proposed chromatic aberration retrieval algorithm in a real-world scenario, we applied the method to a small-scale laboratory setup. This test bed was previously built to generate and measure chromatic aberrations with a method that utilizes a 2-D grating to simultaneously disperse spectral components and provide focus diversity.[3] For consistency with Ref. 3, we represent angular and axial dispersion in terms of pulse-front delay (PFD), and radial group delay (RGD), respectively.

The conceptual layout of the experimental setup is shown in Fig. 3(a). A Superlum SLD-52 superluminescent light-emitting diode (SLED) served as a broadband light source, having a bandwidth of approximately 100 nm and spectral distribution of intensity shown in Fig. 3(b). Given the large bandwidth of the source, significant chromatic dispersion can be introduced with a pair of lenses (L1 and L2), which together provided γ = 10.0 fs of RGD. A fused-silica wedge (W) with a 1° apex angle imparted β = 2.5 fs of PFD. Images of the PSF were captured by a camera, which was translated along the optical axis to provide focus diversity.

The focal sweep was performed first with a Semrock narrowband filter (F) with a FWHM bandwidth of less than 7.2 nm and a central wavelength of 1.03 μm to provide images that were effectively monochromatic; in the second sweep the narrowband filter was replaced by a neutral-density filter. From the spectrally filtered images, we measured the monochromatic contribution to the wavefront without the risk of confounding effects from dispersion. The nonfiltered set of PSF images exhibited a very subtle blurring effect due to dispersion and the increased bandwidth. Because these effects are subtle, the dominant monochromatic wavefront was first estimated in terms of Zernike coefficients; then the dispersion was retrieved in terms of tip, tilt, and focus coefficients that vary linearly with wavelength. Lastly, all of the variables were jointly optimized to produce the final estimate.

The final pupil wavefront estimate, shown in Fig. 3(c), differed by only 16.9-nm rms from the monochromatic result. The final dispersion estimate consisted of 4.68 fs of PFD and 9.13 fs of RGD, which differ by 6.4% and 8.7% from the expected values of

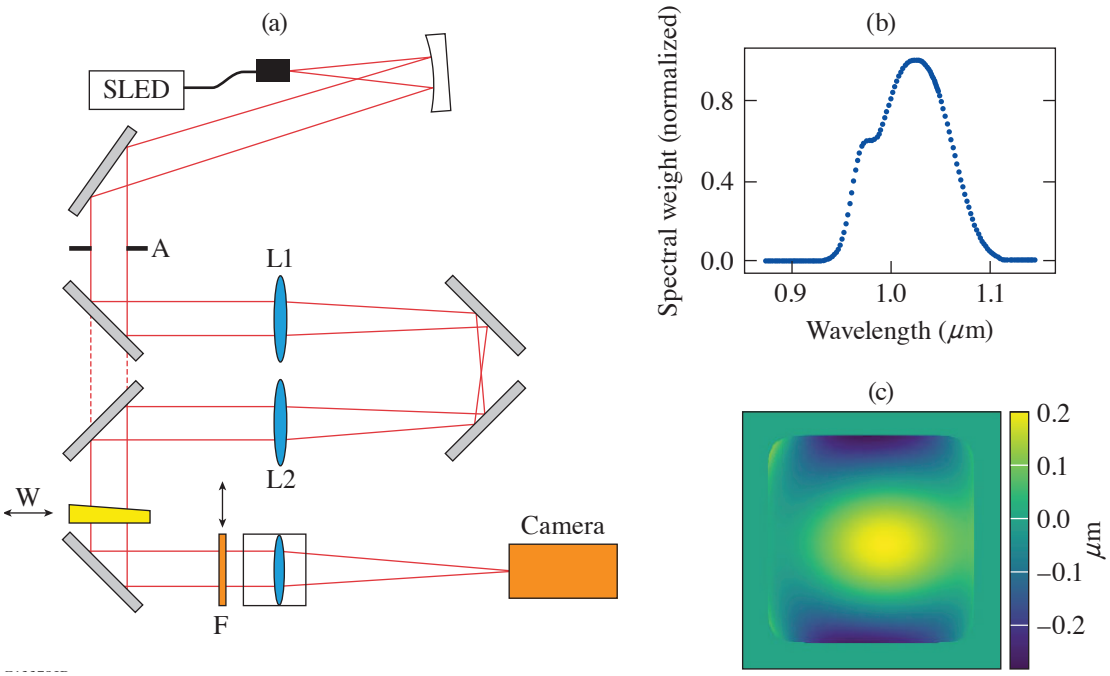

Figure 3
Laboratory experiment setup and results: (a) Experimental system layout (reprinted from Ref. 3); (b) intensity spectrum of the SLED; and (c) final wavefront estimate (full bandwidth). A: apodizer.

5.0 fs and 10.0 fs, respectively. Compared to the results in Ref. 3, where the PFD estimate was within 0.5 fs of expectations and the RGD within 0.1 fs, these results for PFD are similar, while the RGD is less accurate.

In summary, we have developed a simulation model and optimization process for the joint estimation of linear chromatic aberrations in addition to monochromatic aberrations using a measured broadband PSF together with a known aperture, spectrum, and initial wavefront estimate. We found a bootstrapping strategy that first estimated the monochromatic wavefront correction followed by optimization of the chromatic parameters to be highly successful. A test of this approach in a laboratory experiment produced encouraging results.

This material is based upon work supported by the Department of Energy National Nuclear Security Administration under Award Number DE-NA0003856, the University of Rochester, and the New York State Energy Research and Development Authority.

1. J. R. Fienup, Appl. Opt. **21**, 2758 (1982).
2. B. E. Kruschwitz *et al.*, Opt. Express **20**, 20,874 (2012).
3. S.-W. Bahk, C. Dorrer, and J. Bromage, Opt. Express **26**, 8767 (2018)